

Atomistic Mechanisms of Sliding in Few-Layer and Bulk Doped MoS₂

Enrique Guerrero^{†*} and David A. Strubbe^{†*}

[†]*Department of Physics, University of California, Merced, Merced, CA 95343*

E-mail: eguerrero23@ucmerced.edu; dstrubbe@ucmerced.edu

Abstract

Sliding of two-dimensional materials is critical for their application as solid lubricants for space, and also relevant for strain engineering and device fabrication. Dopants such as Ni surprisingly improve lubrication in MoS₂, despite formation of interlayer bonds by intercalated Ni, and the mechanism has remained unclear. While sliding on the atomistic level has been theoretically investigated in pristine 2D materials, there has been little work on doped forms, especially for the complicated case of intercalation. We use density functional theory to study sliding of Ni-doped MoS₂, considering Mo/S substitution and octahedral/tetrahedral intercalation. We find that bulk and trilayers are well described by pairwise bilayer interactions. Tetrahedral intercalation between layers dramatically increases their sliding barrier, but minimally affects sliding between adjacent undoped layers, thus preserving effective lubrication. We provide an atomistic view of how sliding occurs in doped transition-metal dichalcogenides, and a general methodology to analyze doped sliding.

MoS₂ is a semiconducting transition metal dichalcogenide (TMD) with low-friction lubricative properties due to the ease of shearing of its lamellar structure,¹ and is often used for space applications.^{2,3} Sliding can also be important for strain engineering,⁴ nanoelectromechanical systems,⁵ oscillators,⁶ sliding ferroelectrics,⁷ and assembly of twisted bilayer

structures.⁸ For all these applications, it is important to understand how the atomistic mechanisms of slip which are understood in bulk materials are modified on the nanoscale for sliding in novel 2D materials, and especially how dopants influence sliding. MoS₂ can be doped to tune the electronic properties,⁹ increase the catalytic activity,^{10,11} improve lubrication,^{1,12} or change the layer dependence of friction.¹³ Friction in two-dimensional (2D) materials like MoS₂,^{14–18} graphene,^{17,19} and hexagonal boron-nitride (hBN)^{20,21} has been simulated using models of varying complexity, but computational studies of doped materials are rare, so far only for intercalated graphite²² and substituted hBN.²¹ Sliding in doped TMDs, doped bulk 2D materials, or transition-metal-doped 2D materials does not seem to have been studied computationally. The usual approach for exploring sliding in 2D materials is through the sliding potential-energy surface:²³ energies are computed as a function of sliding displacement, and the effect of variables such as load or layer orientation can be examined. In these van der Waals (vdW) mediated systems, a consensus has formed that the interfacial geometries and resulting charge density fluctuations are primarily responsible for the sliding potential’s shape.^{14,17,21,24} This idea has been used as the basis for a classical approximation of the potential.^{20,25} The sliding potential has been shown to be altered by S corrugation from layer rotation¹⁴ or introduction of vacancies,²⁴ which can also happen by formation of distorted 1T phases.²⁶ This picture based on weak vdW interactions could be altered when there are dopants between layers,^{15,27} such as in intercalation of Ni²⁸ or Re²⁹ where the dopants form covalent interlayer bonds. Dopants, especially intercalated dopants, introduce local bond strain and atomic mobility which must be carefully considered during computation and analysis when compared to the standard approach. Ni increases the degrees of freedom, meaning we have to balance relaxing the local structure and preserving a quantifiable sliding amount. Previous simplifying methods like the registry index²⁵ are not easily applicable with intercalation where significant structural changes (e.g. bond changes) can occur. Finally, choices in the initialization of structures in independent computations can affect the final result and lead to pathway discontinuities.

Previous sliding studies have extended to bilayers with vacancies.^{24,30} Like dopants, vacancies could introduce local bond reorganization which must be considered. Vacancy complexes as large as seven atoms were found to universally reduce the sliding barrier while leaving the potential's shape unaffected.²⁴ Dissociated H₂O's between layers has been found to severely diminish lubrication.¹⁵ Conversely, Cheng et al. consider carbon doping in hexagonal boron-nitride bilayers with DFT. C's presence was shown to decrease the friction for substitution of either B or N²¹—the interlayer interaction is weakened by the dopant and thus lubricity is improved. By contrast, calculations showed that Li intercalation in graphite greatly increased barriers to sliding, due to electrostatic interactions after charge transfer from Li to semimetallic graphene layers.²² We have previously computed that Ni-doped MoS₂ does not reduce the binding energy between adjacent layers as Li might do³¹ but rather increases it substantially in t-intercalated doping,³² opposite to what was found for C-doped BN. While intercalated Li can be thought of like ball bearings that decouple MoS₂ layers and would reduce friction (though surprisingly it is not clear this effect has been measured), intercalated Ni instead increases the coupling between MoS₂ by bonding. Ni has been found to not significantly alter MoS₂'s friction and enhance its resistance to wear, or layer flaking,^{12,33} and may have promise for increasing the capabilities of lubrication in space.² This is consistent with the idea that Ni-doping improves MoS₂'s resistance to wear (material loss through flaking) but appears counter to the idea that Ni doping improves lubrication.^{12,33} Calculations of Graphene/Fe₂O₃ interfaces with B, P, Si, and S dopants have found a frictional reduction. These defective cases do not consider the possibility of geometrical reorganization during sliding beyond the out-of-plane direction.¹⁴ While that direction is likely the most energetically important, local bond distortions could occur at the defect sites during sliding and alter the sliding potential.

Ni has been found to improve MoS₂'s lubrication performance,³³ enhance MoS₂'s catalytic activity, and alter the electronic properties.²⁸ We have previously computed four potential Ni dopant sites to MoS₂:^{28,32} Mo substitution, S substitution, tetrahedral (t-) intercalation

and octahedral (o-) intercalation and consider all of them in this work. In this article, we use density functional theory to explore how the presence of Ni modifies potential-energy surfaces and structures during sliding under different atomic constraints. We consider the Ni dopant locations in Fig. 1 and find the relation between bilayer sliding and bulk shearing. We provide insight and methods for analysis generally applicable to sliding of doped 2D materials.

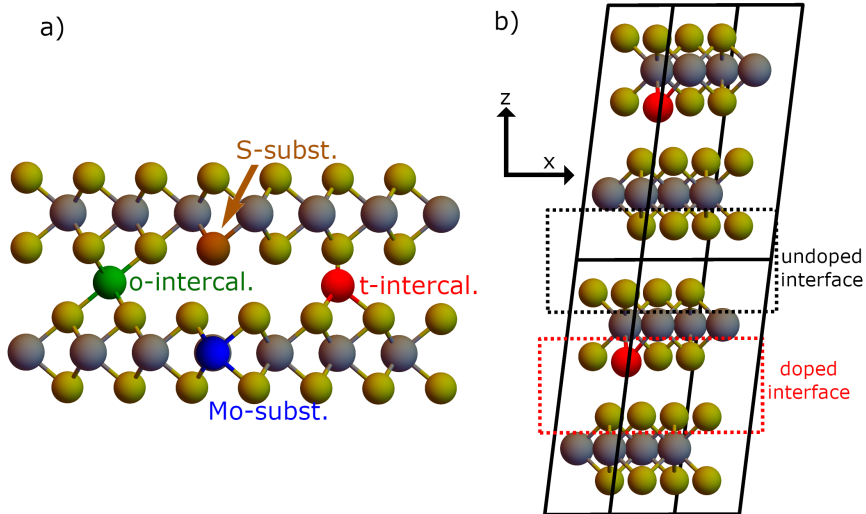


Figure 1: a) The four dopant sites considered in this work, previously found to be stable or metastable.²⁸ Bilayer and bulk structures with similar atomic coordinates are computed. b) A sheared S-substituted cell showing two distinct interfaces in each bulk cell.

We begin with doped and pristine 2H-MoS₂, in the AA' stacking.²⁵ Initial structures are generated by fully relaxing doped bulk structures, then forcing hexagonal symmetry onto the cell (relaxed cell angles differ from the pristine 120° by at most 0.025°, and energies differ by 10⁻⁴ eV/atom). Our coordinate system has the x -axis in the zigzag direction and y -axis in the armchair direction. The top layer is then displaced in the x -direction by Δx in steps of 1/12th of the cells' respective lattice constant a . a was set to 3.19018 Å, 6.39945 Å, 6.38666 Å, 6.35100 Å, and 6.39413 Å for pristine, Mo-substituted, o-intercalated, S-substituted, and t-intercalated in both bulk and bilayers. In bulk, the x -component of the out-of-plane vector c_x was set to $2\Delta x$, such that every pair of layers experienced relative sliding of Δx . In intercalation, Ni was moved along with the mobile top layer, since it was

closer to the intercalant. Substitutional Ni was moved along with the layer it is in. Energies are computed by a self-consistent field (SCF) computation and then the structure is relaxed by three successive levels of constraints as summarized in Fig. S1. (1) Atoms are allowed to relax in the x -direction and the c_z lattice parameter is relaxed (z -relax). (2) Atoms are further relaxed in their y -coordinates (yz -relax). (3) Atoms are further still relaxed in x (xyz -relax). Throughout stages (1)-(3), the Ni atom is allowed to relax in all coordinates so as to capture its preferred movement throughout sliding.

Each constraint gives us different information about the structure throughout sliding. z -relax yields the 1D-sliding potential as it relates to interlayer distances. yz -relax allows us to access the 2D-sliding potential and find deviations from the low-barrier sliding pathway. xyz -relax allows us to test whether shearing occurs like a deck of cards or with the presence of slip planes. Furthermore, the initial structure after sliding but before relaxation can be thought of as stage (0), no relaxation. A similar data set was constructed for y -direction sliding and can be found in the Supplementary Information.

It is important to relax the Ni atom's position during intercalated sliding because the local geometry is expected to change when it experiences different local environments. Ni bonding remains at 6 and 3 bonds for Mo-substituted and S-substituted sites throughout sliding respectively, but bonds form and break for intercalated sliding. Given full relaxation freedom in xyz -relax, both structures follow paths with four Ni-bonds, indicating the high stability of that bond configuration.

The sliding potential in both bulk and bilayer shows a mirror symmetry in the x -direction. This is because the AA' stacking of pristine, Mo-substituted, S-substituted, o-intercalated, and t-intercalated belongs to symmetry point groups D_{6h} , D_{3h} , C_{3v} , C_{3v} , and C_{3v} respectively, which include this mirror symmetry. Moreover, interlayer sliding in the x direction transforms as the function xz , which in each point group belongs to an irreducible representation other than the totally symmetric one; therefore the forces are zero along the sliding direction at AA' and other high-symmetry points. In pristine, this information can be used

to reduce the computational workload, but once the doped structure is relaxed, there is slight symmetry-breaking in all doped cases, quantified in Fig. S9. Since every interface involves at least one pristine layer, the symmetry of the full sliding potential shows hexagonal symmetry.

Results of z -relax in Fig. 2 show that the sliding barrier is massively increased in t -intercalation, unlike previous results with vacancies.²⁴ As layers slide, the identifiers “tetrahedral” and “octahedral” are used to describe the initial structure prior to sliding, despite the fact that bond count and orientation change. The difference between t - and o -intercalations’ energetic response to 1D-sliding can best be explained by changes in their bonding, (See Fig. S2) where o -intercalation is allowed to move into the more stable 4-bonded configuration while t -intercalation is forced to increase its bonds to 5 or 6. Fig. 2b separates c_z into the two interlayer distances present in a cell. These distances are the same for pristine and Mo-substitution, where every other interface is equivalent, but are not for the other structures. This leads to the surprising result that t -intercalated and S-substituted structures attempt to keep their interlayer distance where the Ni is between two layers. This propensity for the interface in these sites to remain similar throughout sliding suggests that the slip planes occur away from the dopant site.

In y -relax, the structures are free to follow a curved path indicative of the familiar zigzag sliding pattern^{14,25} of hexagonal lattices. This curved path is quantified as Δy , the mean difference in Mo y -coordinates when compared to the $\Delta x = 0$ Å structure after relaxation. The white circle in Fig. 3 represents the metastable AB_1 (Mo eclipses Mo) stacking of the pristine structures. Besides t -intercalation, doped structures follow a pathway to equivalent sites through the same metastable site. The t -intercalated structure instead relaxed to a stacking equivalent to the lowest-energy stacking, causing discontinuities in Δy at $\Delta x = 1.6$ Å in Figs. 3 and S2. This is likely due to the deep well at the equivalent stable stacking to attract our system to that configuration, and small barriers could be overcome by the BFGS quasi-Newton algorithm as implemented in ESPRESSO.³⁴ In Fig. 2, we included a structure

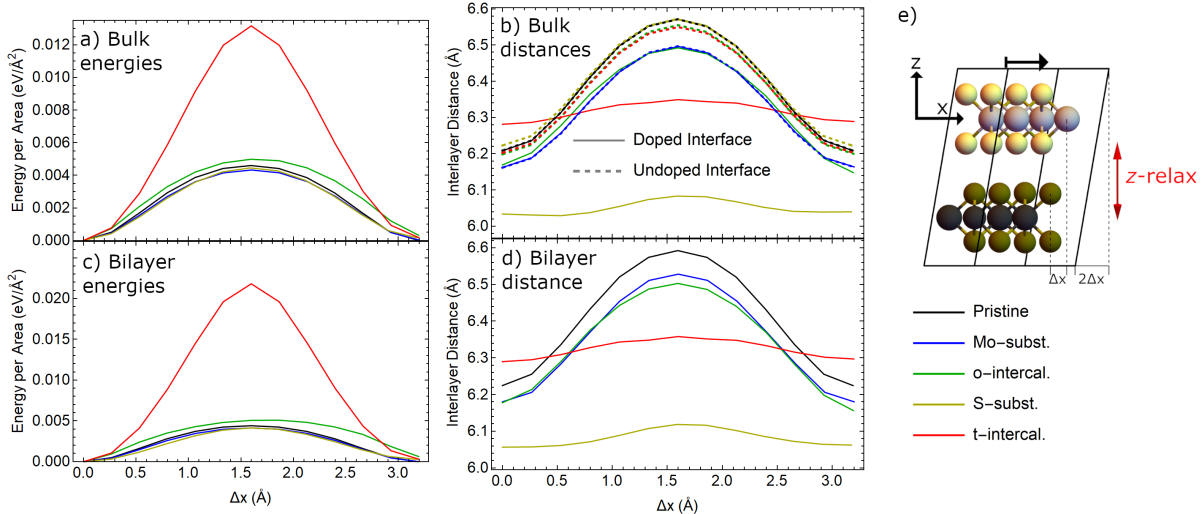


Figure 2: Energies and interlayer distances for x -sliding after z -relax conditions were applied as in e). Energies for a) bulk and c) bilayer shown are divided by the areas of the actively sliding interfaces (i.e. $2 \times$ cell's area in bulk, once in bilayer). Interlayer distances in b) are compared between doped (solid) and undoped (dashed) interfaces. S-substitution and t-intercalation show the largest difference between the two, where they have a strong preference to keep the interlayer distance the same. d) Bilayer distances are similar in shape to bulk.

computation which follows the trends better, but was obtained by altering the relaxation scheme. It was initialized by sliding a nearby structure, rather than sliding the initial AA' structure. Furthermore, both intercalated structures deviate slightly in their sliding pathway due to forces from the Ni-S bonds. The results of this method are reminiscent of what may be achieved through the nudged elastic band method,^{15,35} though we do not require the images to remain close by. This method accesses the 2D-sliding path by simply allowing the system to 'fall' into low-energy pathways in the potential energy surface. Given the complexity introduced by local atomic organization, this analysis approach can capture the concerted relative sliding of layers but also allowing for local symmetry breaking with relaxations of atoms nearby the Ni atom. Along the zigzag sliding path, S-substituted layers attract the opposite layer during sliding (Fig. 3b), as we also found when applying increasing loads in Fig. S8. For y -sliding in Fig. S6, we instead use xz -relax conditions, but we found that the structure did not deviate from a straight path along the y -axis due to mirror symmetry in the xz -plane which is preserved for displacement along the y -axis.

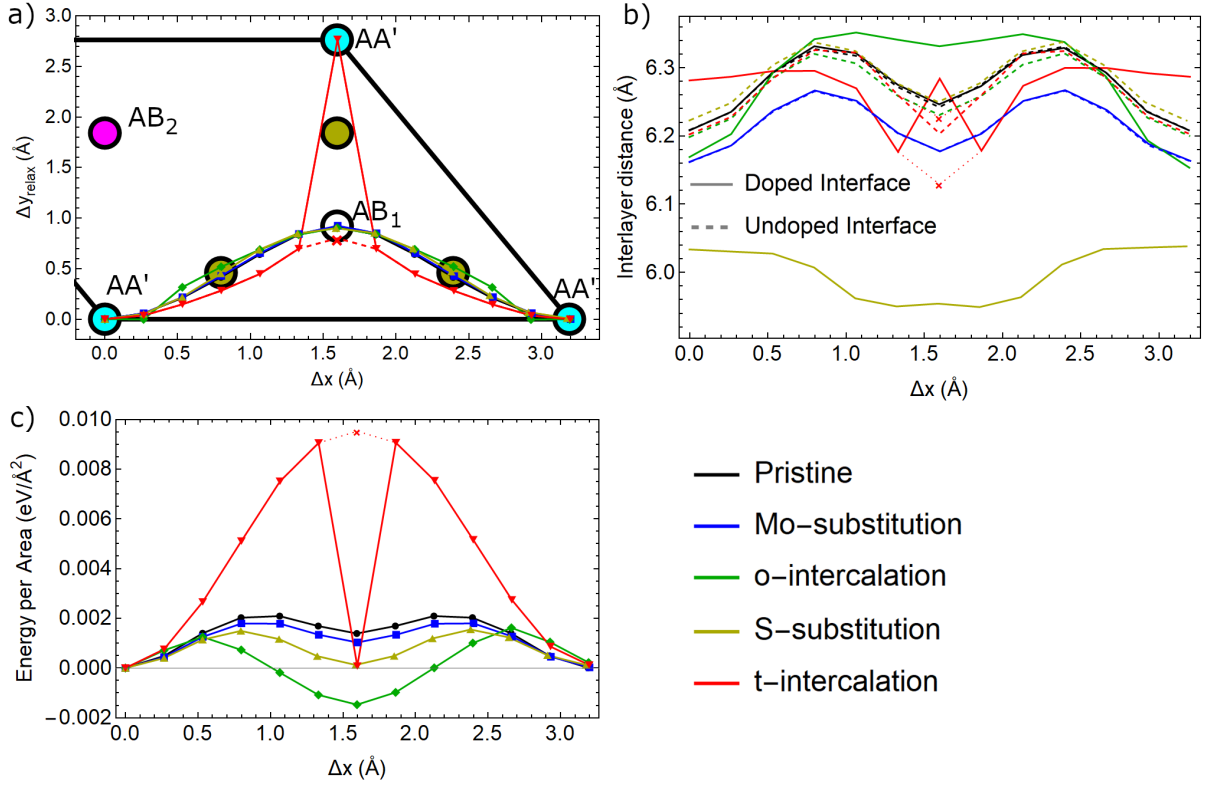


Figure 3: Structure and energy of bulk sliding layers by Δx then relaxing in y and z coordinates. a) The relative displacement after relaxation. Colored circles indicate high-symmetry stackings as labeled, except that the yellow/brown circles mark the locations of energy extrema for S-substitution. Given the opportunity to relax in y , structures traversed the potential surface between stable and metastable stackings. b) Mo-Mo interlayer distances are shown for both doped and undoped interfaces. S-substitution, unlike others, does not increase its doped interface's interlayer distance, indicating an attraction between the dopant and its opposite layer. c) Energies along the sliding path are displayed as well. For b)-c), a red \times indicates the t-intercalated structure as generated by a different scheme than other structures to target the AB₁ stacking.

We use the least restrictive constraint, *xyz-relax*, to detect preferred locations of slip-planes. Fig. 4a shows Δx_{relax} , the average difference between *x*-coordinates of Mo atoms of the two relaxed layers in the cell with respect to Δx with AA' stacking. By sliding the layers uniformly and shearing the cell then relaxing along that same sliding direction, we can see whether it is favored to have uniform relative displacements between layers, more displacement between doped interfaces, or less displacement between doped interfaces. For pristine and Mo substitution, the two interfaces are identical by symmetry and must have the same displacement, but other structures break this symmetry and can have different displacements. The t-intercalated interface shows a strong preference for the AA' stacking. Conversely, S-substituted and o-intercalated interfaces prefer the metastable stacking. This suggests that these structures show a preference to the slip plane shown in 4b, but larger supercells in the *z* direction are required to break the Mo-substituted symmetry and test its slip-plane preference directly.

To that end, we compute a few bulk supercells with 4-layers but only one doped layer in (Fig. 4c-d) (note this has half the Ni concentration of our structures thus far). Both Mo-substitution and t-intercalation relax to alternative stacking configurations rather than the input uniform sliding. We compute the Δx_{relax} of the four interfaces, or pairs of layers, and contrast the behavior of interfaces involving *vs.* not involving the dopant. We find doped Mo-interfaces absorb the sliding, while the undoped interfaces attempt to remain in AA' stacking. At around 0.5 and 1.2 Å, instabilities due to small energy differences in layer orientation emerge, but the undoped interface ultimately remains closer to AA' stacking. Conversely in t-intercalation, Δx_{relax} stays near 0 Å throughout sliding for the doped-interface, just as in the two-layer per cell structure in Fig. 4a. Pristine structures, even when perturbed, relax to a uniform shearing as in Fig. 4b. This study locates the slip plane at the doped interface for Mo-substitution (as in Fig. 4b iii) and away from the interface at t-intercalation (as in Fig. 4b ii). The in-plane lattice is not relaxed.

The bulk structure we have shown thus far contains two interfaces within each cell and

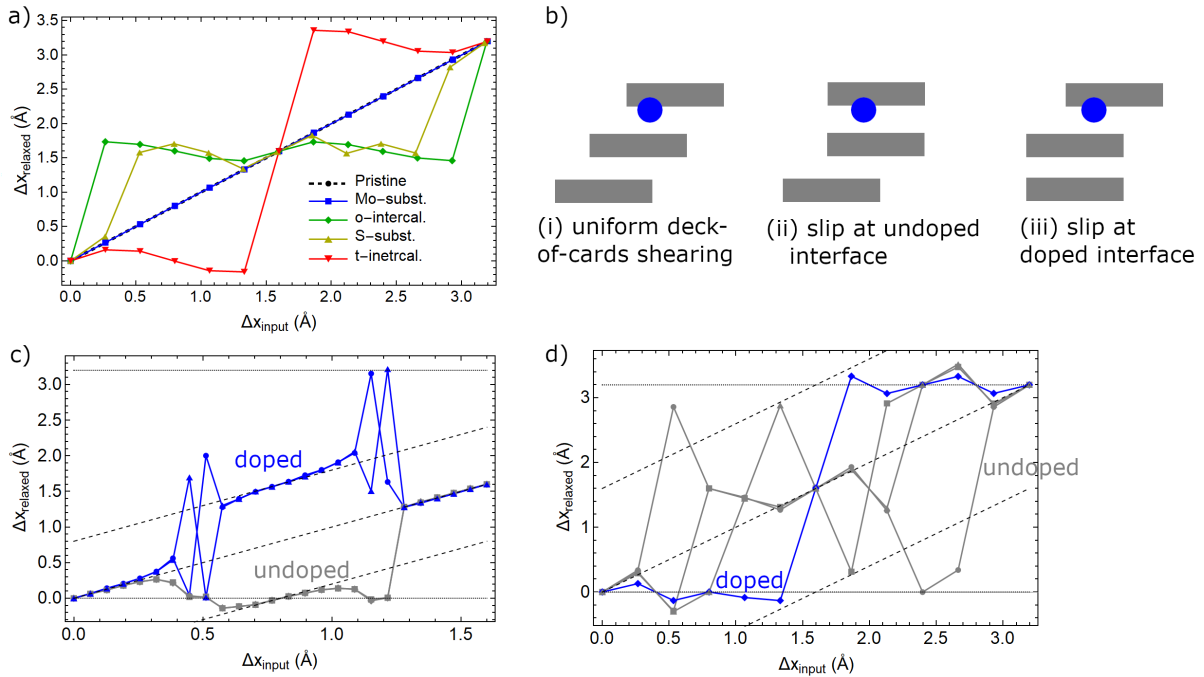


Figure 4: Geometry after bulk shearing in x by Δx then relaxing in x , y and z coordinates. a) The relaxed sliding distance Δx_{relax} as a function the input sliding distance Δx with 2 layers per cell. b) A schematic of potential multilayer slip-plane configurations. c) Mo-substituted and d) t-intercalated interlayer x displacements, $\Delta x(\text{relax})$ for doped (blue) or undoped (gray) interfaces in bulk structures with four layers per cell.

have a concentration of one Ni per 8 MoS₂ units. To understand the range of interactions and quantify how well this may match other concentrations of dopants, we computed an isolated bilayer system with the same initial atomic coordinates as in bulk, but with vacuum in the c direction. Relaxing such structures with identical constraints yields the same stacking configurations found in the bulk. This leads to the intuitive result that the interlayer interactions in the bulk structure can be computed as pairwise interactions of bilayers as summarized in Fig. 5—effects are local to the layers, van der Waals and covalent, not modified by farther away or electrostatic charge transfer. This coincides with comments that the interfacial geometry,¹⁷ and not any deeper structures, are almost entirely responsible for the shape of the sliding potential. As shown in Fig. 5, the practical result is that we can construct the bulk sliding energies by summing up appropriate sliding potentials of bilayer computations. Namely, bulk o-intercalation, t-intercalation, and S-substitution potentials are sums of their bilayer counterparts and the pristine computation while bulk Mo-substituted and pristine are twice their bilayer counterpart potentials. Fig. 5d, for example, has two interface interactions in our bulk structures, one interface with no Ni atom and one with the Ni atom—so we approximate it by summing up a pristine bilayer sliding potential and the t-intercalated bilayer sliding potential to remarkable accuracy. In effect, this leads to the conclusion that arbitrary layered structures can be computed as an appropriate ensemble of bilayer computations that match the interfacial geometry. Work by Hu *et al.*¹⁶ studied sliding in 5-layer systems using classical potentials. Such a study would be expensive using density functional theory due to the large number of atoms, but could be reduced in cost dramatically while achieving DFT-level accuracy by careful combination of four bilayer computations representing the interfaces.

To directly test the localization of the interaction at the interface, we computed a few trilayer scenarios. The top two layers were pristine in all scenarios. The third layer is initially attached to the middle layer and is set to either t-intercalated, Mo-substituted, or pristine. We treat the system up to yz -relax only. We find that the bottom pair of

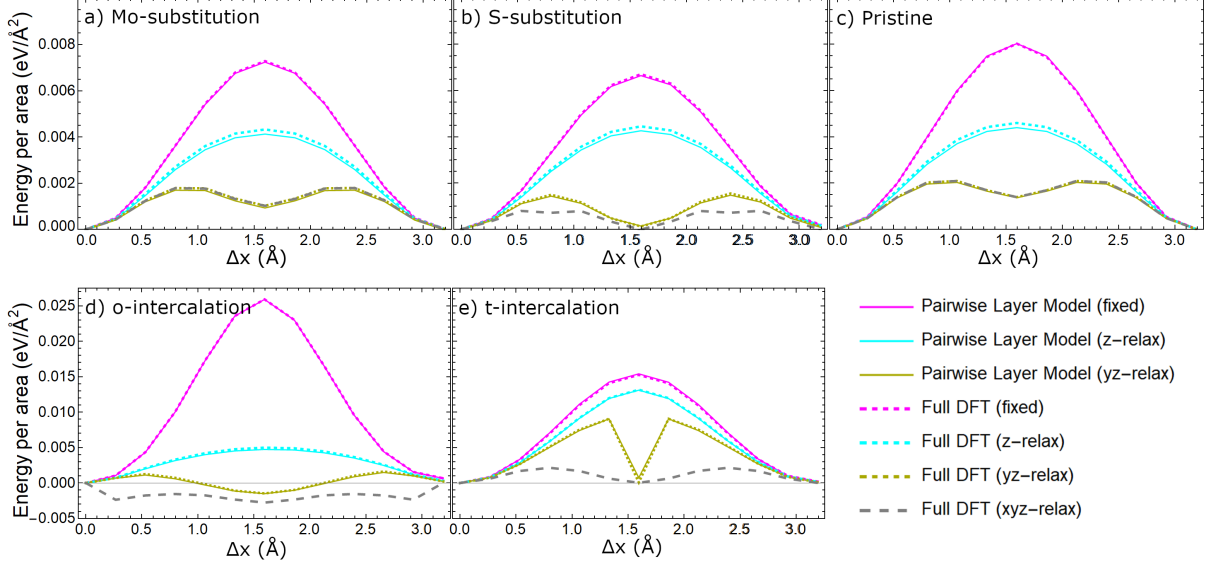


Figure 5: The computed (dashed) variation in sliding potential in bulk plotted against sums of bilayer sliding potentials (solid). Bilayer structures whose interfaces match those in bulk are used: two Mo-substituted/undoped bilayer interactions generate one bulk Mo-substituted sliding potential, others are sums of one undoped interface (i.e. pristine bilayer sliding) and one doped interface. The approximation would only be suitable for xyz -relax conditions if a full 2D sliding potential is computed, since relaxing bilayers in all coordinates yields AA' stacking.

layers remain in the AA' stacking throughout sliding in all conditions. The top pair of layers follow an identical trajectory as the pristine bilayer and the sliding potential per area is indistinguishable in all three scenarios, corroborating that only the active interface contributes to the sliding potential of 2D materials. As a lubricant, Ni-doped MoS_2 shows higher resistance to wear and lower friction than pristine MoS_2 . Given the increased sliding potential maximum of t-intercalated MoS_2 when compared to pristine, one may be tempted to assume the increased lubrication incompatible with t-intercalation. Our result subverts that expectation. With previous computations of the dissociation energy,³² t-intercalation may bind the layers therefore decreasing the wear rate. Slip in t-intercalated MoS_2 can occur at the undoped interface, avoiding high-barrier t-intercalated sliding and relegating all of the sliding to undoped interfaces.

This work elucidates the atomistic mechanisms of doped 2D materials and outlines a systematic pathway to study systems with otherwise large degrees of freedom. The analysis

pathway used is applicable to any layered material and at computational levels other than DFT, though an adequate model of the vdW interaction is critical for accuracy. Given that the pairwise bilayer interactions accurately describe the bulk, arbitrarily-layered systems could be discretized and computed as bilayers that represent each interface. This could reduce computational cost while keeping accuracy of many-layered studies.¹⁶ The variable constraint method used here can be used to simplify the complicated structures with dynamic internal components, such as in S-substituted or intercalations. We used these to find a low-barrier sliding path, compare the Ni’s site-dependent alterations to the sliding potential, and locate the likely slip planes in those structures. A potentially perplexing result that t-intercalation has a large sliding potential and yet can lead experimentally to lower friction can be explained as the presence of shear planes away from intercalated layers. Our results provide general insight into sliding of doped 2D materials, for use in applications and for tuning sliding interactions in 2D materials, and our work offers a general approach for analysis, including for mapping out sliding potential energy in 2D.

Methods

We use the plane-wave DFT code Quantum ESPRESSO³⁶ version 6.6 to compute the properties of bilayer and bulk Ni-doped MoS₂, as in our previous work.^{28,32} We use the Perdew-Burke-Ernzerhof (PBE)³⁷ exchange-correlation functional and Grimme-D2³⁸ (GD2) vdW corrections to capture the weak interactions which mediate the sliding potential in pristine MoS₂. We use optimized norm-conserving Vanderbilt (ONCV) pseudopotentials³⁹ as parameterized by PseudoDojo.⁴⁰

$2 \times 2 \times 1$ supercells of the 6-atom unit cell were used with one Ni atom per cell. Half-shifted Monkhorst-Pack k -grids were used, with in-plane sampling of 6×6 for pristine 4×4 for doped cells, and an out-of-plane grid size of 2 for bulk and 1 for single or multi-layer structures. Kinetic energy cutoffs of 60 Ry were used. Self-consistent field (SCF) energies

were computed to thresholds of 10^{-8} Ry. Total energies and forces were relaxed to 10^{-6} Ry and 10^{-4} Ry/Bohr. Stress relaxations used thresholds of 0.05 kbar.

Bilayer structures were calculated with a fixed out-of-plane lattice parameter $c = 25$ Å to provide vacuum. Trilayers of pristine and doped structures were constructed by adding a third, pristine layer to the bilayer structure and adding the layer thickness to c . Four-layer out-of-plane supercell bulk structures are extensions of the pristine, Mo-substituted, and t-intercalated bulk structure cells with the dopant kept in only one layer.

The number of bonds to a Ni atom i from neighbors j is defined using the Tersoff bond order function⁴¹ $f_C(r)$, where r is the interatomic distance for a given pair of atoms:

$$N_i^{\text{bonds}} = \sum_{\substack{\text{atoms} \\ j \neq i}} f_C(|\vec{r}_i - \vec{r}_j|) = \begin{cases} 1 & r \leq R - D \\ \frac{1}{2} - \frac{1}{2} \sin\left(\frac{\pi}{2} \frac{r-R}{D}\right) & R - D < r < R + D \\ 0 & r \geq R + D \end{cases} \quad (1)$$

where the bond cutoff $R = 3.2$ Å and the smoothing parameter $D = 0.3$ Å were chosen such that: (1) equilibrium o- and t-intercalated structures have 6 and 4 bonds respectively, (2) equilibrium Mo-substituted and S-substituted structures have 6 Ni-S and 3 Ni-Mo bonds respectively, and (3) variation in numbers of bonds with sliding is reasonably smooth. At equilibrium, the Ni-S bond lengths are 2.38 Å, 2.12 – 2.17 Å, and 2.36 Å for Mo-substituted, t-intercalated and o-intercalated respectively, while the Ni-Mo bond lengths in S-substitution are 2.68 – 2.78 Å.²⁸

Acknowledgement

This work was supported by the Merced nAnomaterials Center for Energy and Sensing (MACES), a NASA-funded research and education center, under award NNH18ZHA008CMIROG6R. This work used computational resources from the Multi-Environment Computer for Explo-

ration and Discovery (MERCED) cluster at UC Merced, funded by National Science Foundation Grant No. ACI-1429783, and the National Energy Research Scientific Computing Center (NERSC), a U.S. Department of Energy Office of Science User Facility operated under Contract No. DE-AC02-05CH11231.

Supporting Information Available

Summaries of geometries and energies of y -sliding in bulk and bilayer, Ni bonding during sliding, analysis of one interfaces in trilayers, analysis of load at the AA' stacking, and symmetry breaking (PDF).

References

- (1) Vazirisereshk, M. R.; Martini, A.; Strubbe, D. A.; Baykara, M. Z. Solid Lubrication with MoS₂: A Review. *Lubricants* **2019**, *7*, 57.
- (2) Krause, O. et al. High-Precision Cryogenic Wheel Mechanisms of the JWST/MIRI Instrument: Performance of the flight models. Proc. SPIE 7739, Modern Technologies in Space- and Ground-based Telescopes and Instrumentation. 2010; p 773918.
- (3) Babuska, T. F.; Curry, J. F.; Dugger, M. T.; Lu, P.; Xin, Y.; Klueter, S.; Kozen, A. C.; Grejtak, T.; Krick, B. A. Role of Environment on the Shear-Induced Structural Evolution of MoS₂ and Impact on Oxidation and Tribological Properties for Space Applications. *ACS Appl. Mater. Interfaces* **2022**, *14*, 13914–13924.
- (4) Peña, T.; Chowdhury, S. A.; Azizimanesh, A.; Sewaket, A.; Askari, H.; Wu, S. M. Strain Engineering 2D MoS₂ with Thin Film Stress Capping Layers. *2D Mater.* **2021**, *8*, 045001.
- (5) Lee, J.; Wang, Z.; He, K.; Yang, R.; Shan, J.; Feng, P. X.-L. Electrically Tunable Single-

- and Few-Layer MoS₂ Nanoelectromechanical Systems with Broad Dynamic Range. *Sci. Adv.* **2018**, *4*, eaao6653.
- (6) Ye, Z.; Otero-de-la-Rosa, A.; Johnson, E. R.; Martini, A. Oscillatory Motion in Layered Materials: Graphene, Boron Nitride, and Molybdenum Disulfide. *Nanotechnology* **2015**, *26*, 165701.
- (7) Wu, M.; Li, J. Sliding Ferroelectricity in 2D van der Waals Materials: Related Physics and Future Opportunities. *Proc. Natl. Acad. Sci.* **2021**, *118*, e2115703118.
- (8) Lia, M. et al. Precise Control of the Interlayer Twist Angle in Large Scale MoS₂ Homostructures. *Nat. Commun.* **2020**, *11*, 2153.
- (9) Bernardi, M.; Ataca, C.; Palumbo, M.; Grossman, J. C. Optical and Electronic Properties of Two-Dimensional Layered Materials. *Nanophotonics* **2017**, *6*, 479–493.
- (10) Mundotiya, S.; Rupesh, S.; Saha, S.; Kakkar, R.; Pal, S.; Kunzru, D.; Pala, R. G. S.; Sivakumar, S. Effect of Sodium on Ni-Promoted MoS₂ Catalyst for Hydrodesulfurization Reaction: Combined Experimental and Simulation Study. *Energy Fuels* **2021**, *35*, 2368–2378.
- (11) Mao, J.; Wang, Y.; Zheng, Z.; Deng, D. The Rise of Two-Dimensional MoS₂ for Catalysis. *Front. Phys.* **2018**, *13*, 138118.
- (12) Vellore, A.; Garcia, S. R.; Walters, N.; Johnson, D. A.; Kennett, A.; Heverly, M.; Martini, A. Ni-Doped MoS₂ Dry Lubricant Life. *Adv. Mater. Interfaces* **2020**, *7*, 2001109.
- (13) Acikgoz, O.; Guerrero, E.; Yanilmaz, A.; Dagdeviren, O. E.; Çelebi, C.; Strubbe, D. A.; Baykara, M. Z. Intercalation Leads to Inverse Layer Dependence of Friction on Chemically Doped MoS₂. *Nanotechnology* **2022**, <https://doi.org/10.1088/1361-6528/ac9393> (in press).

- (14) Levita, G.; Cavaleiro, A.; Molinari, E.; Polcar, T.; Righi, M. C. Sliding Properties of MoS₂ Layers: Load and Interlayer Orientation Effects. *J. Phys. Chem. C* **2014**, *118*, 13809–13816.
- (15) Yang, Z.; Bhowmick, S.; Sen, F. G.; Alpas, A. T. Microscopic and Atomistic Mechanisms of Sliding Friction of MoS₂: Effects of Undissociated and Dissociated H₂O. *Appl. Surf. Sci.* **2021**, *563*, 150270.
- (16) Hu, C.; Yi, C.; Bai, M.; Lv, J.; Tang, D. Molecular Dynamics Study of the Frictional Properties of Multilayer MoS₂. *RSC Adv.* **2020**, *10*, 17418.
- (17) Wang, L.; Zhou, X.; Ma, T.; Liu, D.; Gao, L.; Li, X.; Zhang, J.; Hu, Y.; Wang, H.; Dai, Y.; Luo, J. Superlubricity of a Graphene/MoS₂ Heterostructure: A Combined Experimental and DFT Study. *Nanoscale* **2017**, *9*, 10846.
- (18) Liang, T.; Sawyer, W. G.; Perry, S. S.; Sinnott, S. B.; Phillpot, S. R. First-Principles Determination of Static Potential Energy Surfaces for Atomic Friction in MoS₂ and MoO₃. *Phys. Rev. B* *77*, 104105.
- (19) Ta, H. T. T.; Tieu, A. K.; Zhu, H.; Yu, H.; Tran, N. V. A First-Principles Study of Impurity-Enhanced Adhesion and Lubricity of Graphene on Iron Oxide Surface. *J. Phys. Chem. C* **2021**, *125*, 4310–4321.
- (20) Marom, N.; Bernstein, J.; Garel, J.; Tkatchenko, A.; Joselevich, E.; Kronik, L.; Hod, O. Stacking and Registry Effects in Layered Materials: The Case of Hexagonal Boron Nitride. *Phys. Rev. Lett.* **2010**, *105*, 046801.
- (21) Cheng, Z.; Zhang, G.; Zhang, B.; Ma, F.; Lu, Z. Tuning the Electronic Structure of Hexagonal Boron Nitride by Carbon Atom Modification: A Feasible Strategy to Reduce Sliding Friction. *Mater. Res. Express* **2019**, *6*, 036306.

- (22) Pang, Z.; Wan, J.; Lu, A.; Dai, J.; Hu, L.; Li, T. Giant Tunability of Interlayer Friction in Graphite via Ion Intercalation. *Extreme Mech. Lett.* **2020**, *35*, 100616.
- (23) Ustunel, H.; Toffoli, D. Tribology at the Atomistic Scale with Density Functional Theory. *Electron. Struct.* **2022**, *4*, 023002.
- (24) Wang, J.; Dongare, A. M. Density Functional Theory Study of Electronic Structure of Defects and the Role on the Strain Relaxation Behavior of MoS₂ Bilayer Structures. *J. Mater. Sci.* **2018**, *53*, 9064–9075.
- (25) Blumberg, A.; Keshet, U.; Zaltsman, I.; Hod, O. Interlayer Registry to Determine the Sliding Potential of Layered Metal Dichalcogenides: The Case of 2H-MoS₂. *J. Phys. Chem. Lett.* **2012**, *3*, 1936–1940.
- (26) Karkee, R.; Strubbe, D. A. Panoply of Doping-Induced Reconstructions and Electronic Phases in Ni-doped 1T-MoS₂. *arXiv:2107.07541* **2022**,
- (27) Chen, X.; Chen, Z.; Jun, L. Critical Electronic Structures Controlling Phase Transitions Induced by Lithium Ion Intercalation in Molybdenum Disulphide. *Chin. Sci. Bull.* **2013**, *58*, 1632–1641.
- (28) Guerrero, E.; Karkee, R.; Strubbe, D. A. Phase Stability and Raman/IR Signatures of Ni-doped MoS₂ from Density Functional Theory Studies. *J. Phys. Chem. C* **2021**, *125*, 13401–13412.
- (29) Guerrero, E.; Strubbe, D. A. Structure, friction, and Raman spectroscopy of Re-doped bulk MoS₂ from first principles. *arXiv:2202.12889* **2022**,
- (30) Yu, Z. G.; Zhang, Y.-W.; Yakobson, B. I. An Anomalous Formation Pathway for Dislocation-Sulfur Vacancy Complexes in Polycrystalline Monolayer MoS₂. *Nano Lett.* **2015**, *15*, 6855–6861.

- (31) Enyashin, A. N.; Seifert, G. Density-functional Study of Li_xMoS_2 Intercalates ($0 \leq x \leq 1$). *Comput. Theor. Chem.* **2012**, *999*, 13–20.
- (32) Karkee, R.; Guerrero, E.; Strubbe, D. A. Enhanced Interlayer Interactions in Ni-Doped MoS_2 , and Structural and Electronic Signatures of Doping Site. *Phys. Rev. Mater.* **2021**, *5*, 074006.
- (33) Stupp, B. C. Synergistic Effects of Metals Co-Sputtered with MoS_2 . *Thin Solid Films* **1981**, *84*, 257–266.
- (34) Fletcher, R. *Practical Methods of Optimization*; John Wiley & Sons, Ltd, 2000; Chapter 3, pp 44–79.
- (35) Zarkevich, N. A.; Johnson, D. D. Nudged-Elastic Band Method with Two Climbing Images: Finding Transition States in Complex Energy Landscapes. *J. Chem. Phys.* **2015**, *142*, 024106.
- (36) Giannozzi, P.; Andreussi, O.; Brumme, T.; Bunau, O.; Buongiorno Nardelli, M.; Calandra, M.; Car, R.; Cavazzoni, C.; Ceresoli, D.; Cococcioni, M.; et al., Advanced Capabilities for Materials Modelling with **QUANTUM ESPRESSO**. *J. Phys.: Condens. Matter* **2017**, *29*, 465901.
- (37) Perdew, J. P.; Burke, K.; Ernzerhof, M. Generalized Gradient Approximation Made Simple. *Phys. Rev. Lett.* **1996**, *77*, 3865–3868.
- (38) Grimme, S. Semiempirical GGA-Type Density Functional Constructed with a Long-Range Dispersion Correction. *J. Comput. Chem.* **2006**, *27*, 1787–1799.
- (39) Schlipf, M.; Gygi, F. Optimization algorithm for the generation of ONCV pseudopotentials. *Comput. Phys. Commun.* **2015**, *196*, 36–44.
- (40) van Setten, M. J.; Giantomassi, M.; Bousquet, E.; Verstraete, M. J.; Hamann, D. R.; Gonze, X.; Rignanese, G.-M. The **PseudoDojo**: Training and Grading a 85 Element

Optimized Norm-Conserving Pseudopotential Table. *Comput. Phys. Commun.* **2018**, *226*, 39–54, <http://www.pseudo-dojo.org/>.

- (41) Tersoff, J. New Empirical Approach for the Structure and Energy of Covalent Systems. *Phys. Rev. B* **1988**, *37*, 6991–7000.